EasyChair Preprint

№ 11397

Methodology of Synthesis Nonlinear Mathematical Model of a Servo

Serhii Kochuk, Artem Nikitin, Hanna Hrinchenko and Ihor Bahaiev

November 27, 2023

Methodology of synthesis nonlinear mathematical model of a servo

Serhii Kochuk [1][0000-0003-1429-2246], Artem Nikitin [1][0000-0001-6830-0710],

Hanna Hrinchenko [2][0000-0002-6498-6142] and Ihor Bahaiev [2][0000-0002-9101-5114]

[1] National Aerospace University "Kharkiv Aviation Institute", Kharkiv 61070, Ukraine
[2] Ukrainian Engineering Pedagogics Academy, Kharkiv 61003, Ukraine
lncs@springer.com

Abstract. The object of study in the article is a miniature electromechanical servo drive (SP), the subject of study is the methods of identification and mathematical description of the SP. The following methods are used: structural modelling, Laplace transform, transfer functions, structural and parametric identification. The aim is to obtain mathematical models of SP as an executive device of mechatronic system (MS) according to the experimental data. Objectives: to develop and identify a mathematical model of SP, which can be used in the design and modelling of MC actuators. The structural representation of the SP as a closed-loop tracking system with negative feedback on the position of the output link is used. It is proposed to extend the passive and active identification of SP as an integral object to the identification of parameters of each element in the device for the subsequent formation of a mathematical model in the state parameters or in the form of structural schemes, to obtain diagnostic models.

Keywords: Servo-Actuators; Mechatronic System; Mathematical Model; Structural Scheme; Timing Characteristics; Transmission Ratio; Time Constant; Transfer Function; Identification.

1 Introduction

Currently, servo-actuators (SA) are utilized as actuating devices such as SG90, MG90, HXT900, etc. in many unmanned systems (US), particularly in small-scale or research robotic, mechatronic, and unmanned aerial vehicle (UAV) systems [1]. For example, in robot models, their number can range up to 8-10 [2], while in UAVs of aircraft type, it is typically 2-4 (see Fig. 1) [3]. These drives exert a significant influence on the dynamic properties of control loops, the reliability of automatic control systems (ACS), and the performance of the object or its model as a whole.

Please try to avoid rasterized images for line-art diagrams and schemas. Whenever possible, use vector graphics instead.

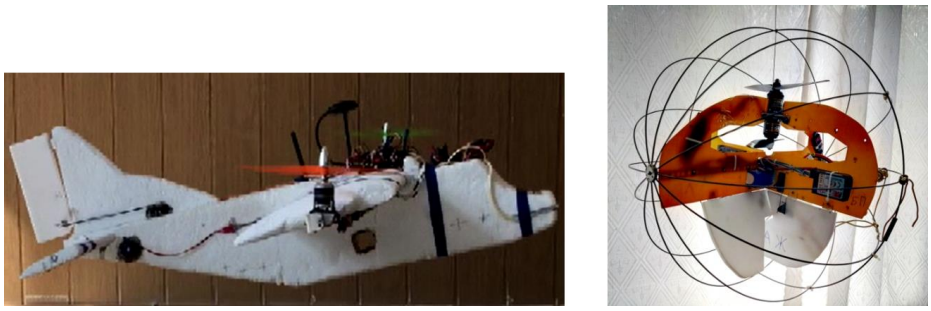

a b

Fig. 1. UAVs with servo-actuators: “B-kopter” (a) and “Vercard” (b).

It is necessary to develop dynamically similar mathematical models of SA of varying complexity for the analysis of the influence of SA parameters on the dynamics, stability, and accuracy of US, as well as for the synthesis of algorithms for their ACS.

2 Problem statement

In most existing US, servo-actuators such as SG90 are often employed without the execution of calculations or their models [5]. However, during the design of US, especially UAV [6], it is important and sometimes necessary to have mathematical models of SA for algorithm synthesis and accuracy assessment of the control system. Flight experiments of a completed model of US with SA in one or several control channels, for example, do not allow determining the impact of servo-actuator's parameters on stability, controllability, and accuracy of control loops. This underscores the validity of the previously proposed comprehensive approach to UAV design [7]. Certain operations with SA [8, 9] engages schematic solutions and properties of driver circuits or motor control boards of actuator but do not delve into the issues of determining parameters of other elements and the servo-actuators as a whole.

The investigation of servo-actuator (SA) characteristics was conducted on the real Micro Servo SG90 (see Fig. 2), which consists of a plastic housing, a direct current motor (DCM), a potentiometer or feedback sensor (FS), a control board (amplifier and comparator), a gearbox, and a wire harness. The transfer coefficients of the control board – k_u (without load and with load), the FS – k_{FS}, and the reduction gearbox – k_r were experimentally determined to formulate a mathematical model of the SA. Based on the extracted static characteristic of the DCM, the parameters of its mathematical model were identified: the transfer coefficient k_{EN} and the time constant T_{EN} in the transfer function of the aperiodic link.

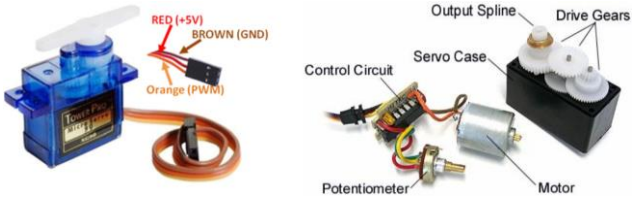

a b

Fig. 2. Servo-actuator Tower Pro SG90 type assembled (a) and disassembled (b).

The experimental setup consisted of a prototype board, Arduino Uno microcontroller, a rotational speed sensor F249 FC-03 [10], and other measuring instruments.

3 Functional and structural diagrams of the servo-actuator

The structure of the SA SG90 closely resembles the widely accepted [11,12] structure of SA as a component of a control system (see Fig. 3): the role of the actuator (A) of the amplifier block, the comparison and feedback formation element (FB) is performed by the control board built based on modules KS5188 or AA5188, the servo unit (SU) is constructed based on the DCM FF-1012VA with magnetic-electric evocation, and the feedback sensor (FS) is implemented using a variable resistor – a potentiometer. The SA includes a three-stage reducer that reduces the revolutions of the motor's output shaft.

The functional diagram of the typical SA SG90 was developed (see Fig. 4) based on the analysis of the interconnections of SA elements.

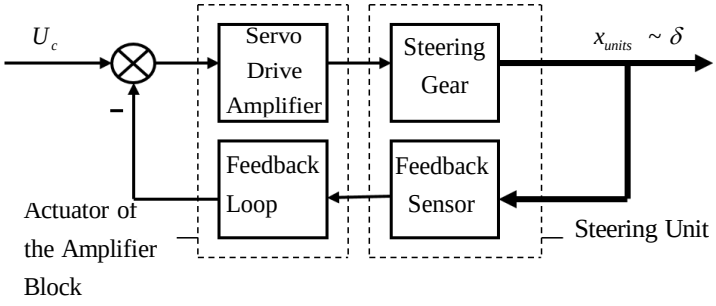

Fig. 3. Typical Structure of a servo-gear.

Mechanical signals are indicated by highlighted lines, while electrical signals correspond to single lines.

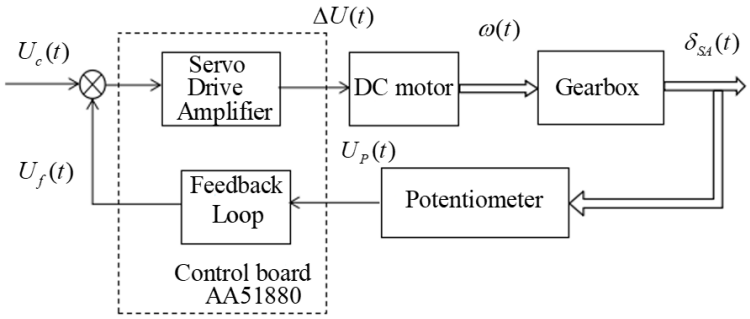

Fig. 4. Functional Diagram of a Typical SA SG90.

The task of further research on the thematic description of elements and the SA as a whole will be to define the input-output functions of each SA element in the form of an equation or transfer function (structural diagram). The structural diagram of the SA can be represented in the following scheme (see Fig. 5).

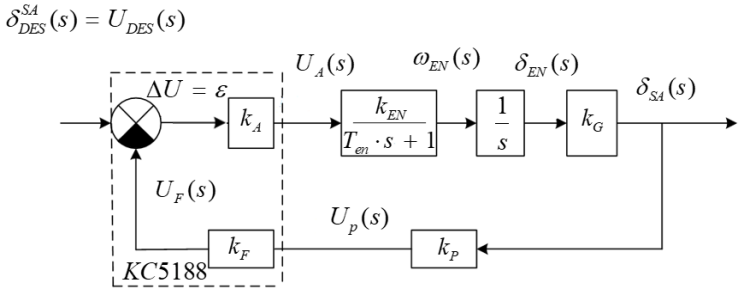

Fig. 5. Structural diagram of the SA.

4 Determining the parameters of servo-actuator elements

The SA was dissected and its components were disconnected from each other during experimental investigation. The operation of some parts (amplifier, motor) was tested both without a load and under load.

4.1 A Subsection Sample

The experimental data of the rotation angle of the potentiometer, PWM signal from the Arduino Uno controller board, and the output voltages of the FS were obtained. Control signals are generated by the controller at a frequency of 20 ms and the maximum voltage signal level is 5 V with a resolution of 1024.

The obtained numbers of N_{PWM} can be transformed into voltages using the formula (1).

$$U_P = f(\delta_{SA}) = N/1024 \times 5 \quad (1)$$

The static characteristic of the potentiometer – FS is presented on Fig. 6.

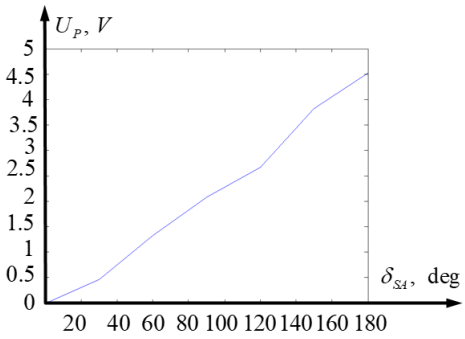

Fig. 6. Static characteristic $U_P = f(\delta_{SA})$.

The averaged transfer coefficient in V/degree of the feedback sensor can be determined from its static characteristic.

4.2 Control Board – Driver

Experimental data of input and output signals (without load and with load, respectively) of the amplifier were obtained, depending on the controlling influence from Arduino Uno. Using a digital oscilloscope, input signals of the amplifier were obtained in the form of PWM pulses which can be converted into voltages using the formula (2).

$$U_{IN}^{AP} = \frac{t}{20 \times 5\ V} \quad (2)$$

The Static characteristics of the SA amplifier are presented on Figure 7 without a load $U_{OUT} = f(U_{IN}^{AP})$ and with a load $U_{OUT}^{L} = f(U_{IN}^{AP})$.

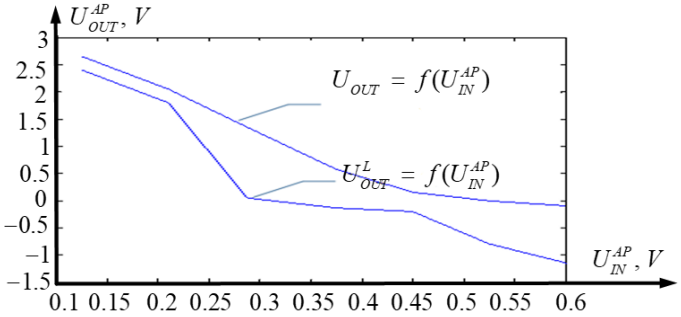

Fig. 7. Static characteristics of the SA amplifier.

The amplification coefficient of the amplifier is determined from the static characteristic without a load $K_{AP} = \frac{2.65 - (-0.1)}{0.6 - 0.125} = 5.79$ and with a load $K_{AP}^{L} = \frac{2.4 - (-1.15)}{0.6 - 0.125} = 7.47$.

4.3 Direct current motor

The speed of the output shaft can be regulated by varying the voltage U_{EN} applied to the armature winding of the DCM. This speed is then transformed into rotational speed and angular displacement through the reducing gearbox δ_{SA}. The motor is connected to a power source capable of smoothly adjusting the voltage within the range from 0 to 5 V with an operational current of 0.1 A for this purpose. The rotational frequency was measured using an optical tachometer and converted into the rotational speed of the motor shaft ω. Experimental data for the DCM for shaft rotation in the counterclockwise (+) and clockwise (-) directions were obtained. This allowed building the diagram depicting the dependence of the DCM rotational speed on voltage (See Fig.8 a). Determination of the coefficient of the transmission ratio from the speed characteristic of the DCM $K_{EN} = \frac{617.53 - 106.76}{1.8 - 0.6} = 425.64$.

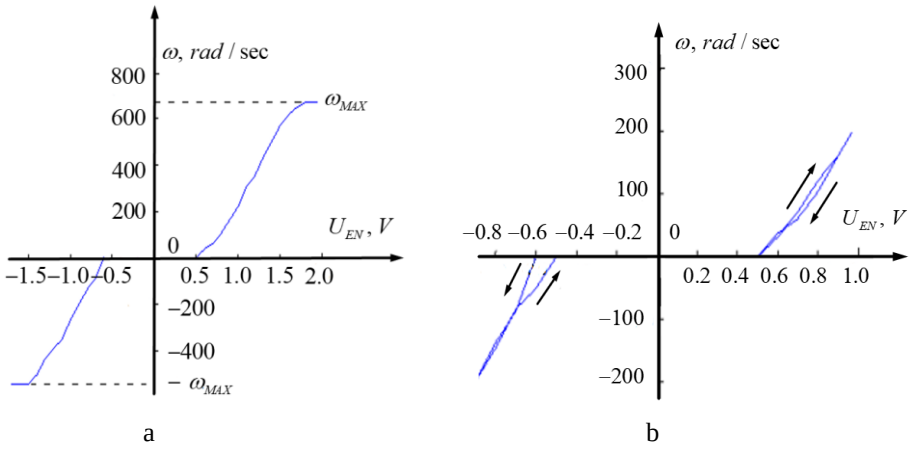

Fig. 8. Speed characteristic of the motor $\omega = f(U_{EN})$ (a), the nonlinearity, such as backlash or hysteresis of the DCM (b).

The DCM has a saturation and insensitivity zone as seen in Figure 8 a. When the voltage exceeds 1.8V (+) or 1.5 V (-), the motor saturates, and the rotational speed no longer changes. The maximum rotational speed values of the DCM without a load are 670 rad/s in the first quadrant (see Fig. 8) and 544 rad/s in the third quadrant. Such asymmetry may be explained by the uneven winding of the three-pole armature winding. The insensitivity zone of the DCM for counterclockwise rotation is $\Delta U_{+} = 0.5, V$ and

for clockwise rotation $\Delta U_{-} = -0.6, V$. The difference in insensitivity zones can be explained by varying resistances in the brush-collector contact areas and the same factors influencing the saturation zone. Relieving the speed characteristic of the DCM in the zone of the insensitivity, depending on the increase and decrease of the voltage on the armature winding U_{EN} , revealed the presence of nonlinearity such as backlash or hysteresis (see Fig. 8 b). This is characteristic of backlash in places where the shaft is seated in the bushings or hysteresis in the armature windings when the motor rotor starts moving.

It is necessary to transfer to the "System Identification Toolbox" in MATLAB to obtain the transfer function of the DCM based on experimental data. The transfer function of the DCM in terms of angular velocity can represent either an oscillatory or inertial link, so it is necessary to compare the two models and choose the better option.

4.4 Reducing gearbox

The Reducing gear box is a mechanical assembly of gears that reduces the rotational speed of the motor and transmits the rotation to the output shaft. The reducing gearbox also contains a pin that limits the maximum angle of rotation.

The reducing gearbox has four gears with the following number of teeth (see Fig.2 b):

$$Z_1 = 8, Z_2 = 48, \; Z_3 = 8, \; Z_4 = 32. \tag{3}$$

The gear ratio or reduction factor is given by:

$$K_R = \frac{Z_2 \cdot Z_4}{Z_1 \cdot Z_3} = \frac{48 \cdot 32}{8 \cdot 8} = 24\,. \tag{4}$$

5 First Section

5.1 The transfer function in the form of an oscillatory element

The transfer function for the angular velocity of a direct current motor with independent or magnetic-electric evocation is represented by an oscillatory element with a damping ratio close to unity or two aperiodic elements in general form. The initial data for determining the type of transfer function and identifying the parameters of the DCM in the "System Identification Toolbox" MATLAB [13] was the speed characteristic of the motor (see Fig. 8). The transfer function of the DCM in the form of an oscillatory element (Model №1) is given by formula:

$$W_{DCM}^{1} = \frac{686.9}{s^2 + 3.434 \cdot 10^{-11} \cdot s + 2.255}\,. \tag{5}$$

The comparison of the static characteristic (5) with the original data of the DCM in the form of the characteristic $\omega = f(U_{EN})$ is presented on Figure 9 a with a match of

97%. A simulation in Simulink MATLAB was conducted to verify this model's functionality

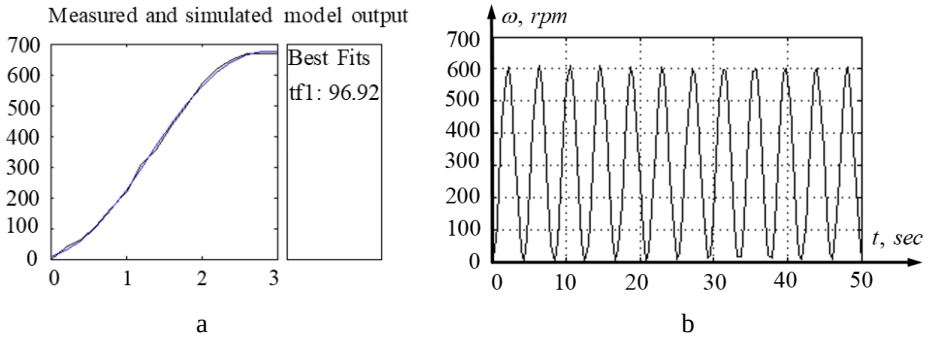

Fig. 9. The comparison of the static characteristic of Model №1 (a), graph of the rotational speed of the DCM of the Model №1 (b)

and the graph of the change in the rotational speed of the DMS's Model №1 when a unit step signal is applied at the input is shown in Figure 9 b.

As seen in Figure 9 b, the step-function response takes the form of undamped oscillations, as the characteristic polynomial contains complex conjugate roots with zero real part (see Fig.10).

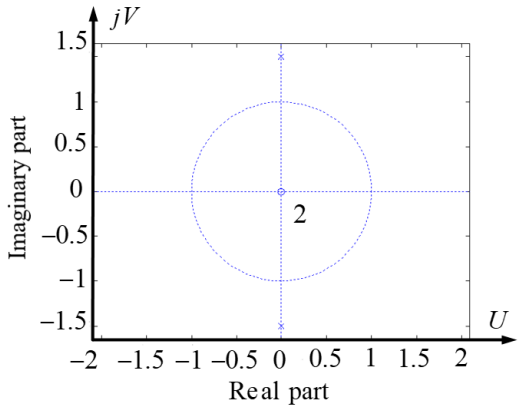

Fig. 10. The graph of the distribution of roots of the Model №1.

Although this model (5) has a very good resemblance to the DCM it cannot be used for further research due to its non-functionality.

5.2 First-order transfer function

The transfer function of the DCM in the form of an aperiodic element (Model №2):

$$W_{DCM}^{2}(s) = \frac{633.3}{s + 1.307} = \frac{484.5}{0.76 \cdot s + 1} \ . \tag{6}$$

Figure 11 a shows the comparison of Model №2 with the original characteristics of the DCM.

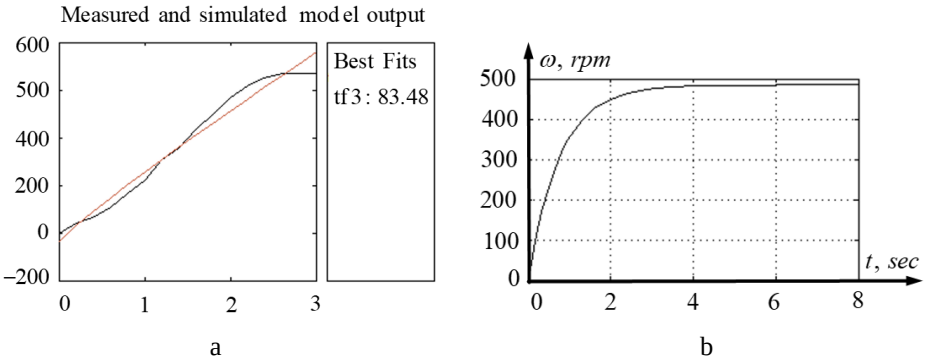

Fig. 11. The comparison of the static characteristic of Model №2 (a), the graph of the rotational speed of the DC motor (Model №2) (b).

Figure 11 b shows the graph of the rotational speed variation for the DCM of Model №2.

The determination of the time constant of the DCM is $T_{DCM} \approx 0.76, sec$ from Figure 11 b. The transient response of Model №2 indicates a practical match of its parameters with the real DCM. Therefore, the model (6) in the form of a first-order lag will be used in further research. After obtaining the transfer function of the DCM, the feedback sensor, amplifier, and reducing gearbox coefficients, a mathematical model of the SA can be constructed in the Simulink MATLAB environment.

6 Synthesis of the Mathematical Model of the servo-actuator

The undetermined parameter in the SA model is the feedback coefficient K_f which will be determined based on the simulation results. The transfer function of the SA as a closed-loop servo system (see Fig. 5) is given by:

$$\Phi(s) = \frac{197.11}{s^2 + 1.307 \cdot s + 0.49} = \frac{402}{1.43^2 \cdot s^2 + 2.67 \cdot s + 1}. \tag{7}$$

The S-model of the servo actuator $K_f = 0.1$ with is presented in Figure 12.

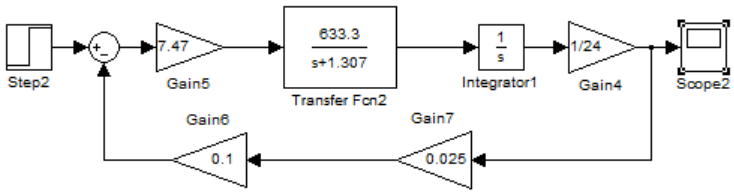

Fig. 12. The graph of the rotational speed of the DC motor (Model №2).

The best performance characteristics are provided by the mathematical model of the SA with overshoot ratio $\sigma = 0 \div 5\,\%$. The error function was used to calculate the overshoot value [14, 15]. For comparison, the graph with the amplifier gain without load and different feedback coefficients is presented in Figure 13.

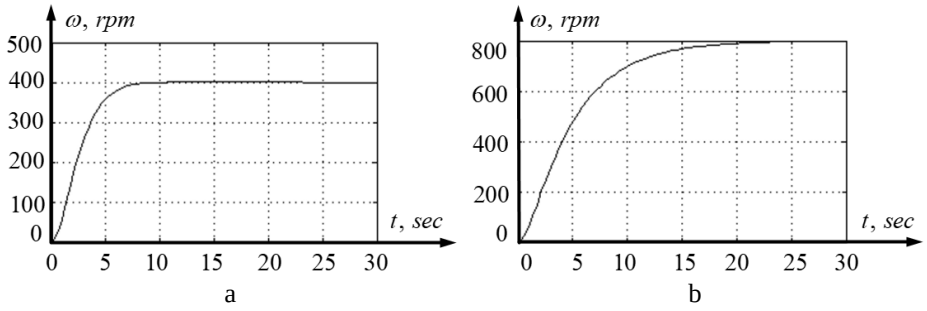

Fig. 13. The graph of ω(t) with $K_f = 0.1$ (a) and $K_f = 0.05$ (b).

The time constants of the SA can be determined from Figure 13. $T_{SA1} = 4.6$ sec when $K_f = 0.1$ and $T_{SA2} = 7.5$ sec when $K_f = 0.05$. The minimum time constant $T_{SA2} = 2.6$ sec is obtained when $K_f = 0.18$ (see Fig.14 a), overshoot ratio in this case $\sigma = 4.84$ %.

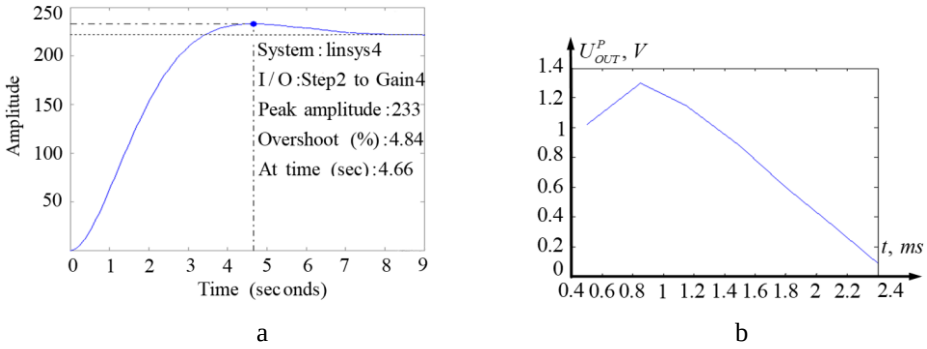

Fig. 14. The graph of $\delta_{SA}(t)$ when $K_f = 0.18$ (a), the static characteristic $U^P_{OUT} = f(t_{PWM})$ (b).

The experimental data of input command (time of pulses in milliseconds), output command from the feedback sensor, and relative angles of rotation of the SA were obtained. $U_P = f(t_{PWM})$ (see Fig.14 b) and SA $\delta_{SA} = f(t_{PWM})$ (see Fig.15 a).

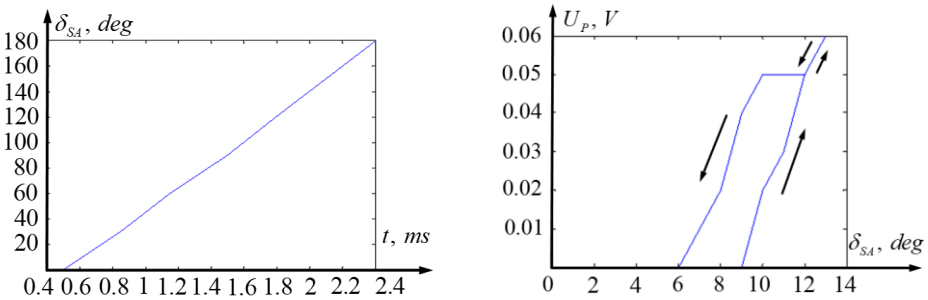

Fig. 15. The static characteristic $\delta_{SA} = f(t_{PWM})$ of the SA (a), nonlinearities of the SA (b).

The closed-loop system also has a dead zone, as shown in Figure 15 a. Let's investigate the behavior of the SA at a small angle range of 6-12 degrees. The dead zone (see Fig. 15 b) is caused by the inertia of the SA's rotor, the presence of resistance in the collector-brush assembly unit, the absence of a bearing in one of the rotor shaft attaching lug nodes (possibly fixated on sliding support), and the magnetic-electric evocation of the motor.

The phenomena of backlash or hysteresis show themselves at a small value due to the properties of magnetization of permanent magnets in the stator and resistances in the rotor attaching lug nodes in the stator housing.

7 Conclusions

Experimental study of SP elements to determine their static and, if possible, dynamic characteristics in order to obtain the structure and refine the parameters of mathematical models for the formation of an adequate computer model of the servo drive as a single mechatronic system has shown the importance of taking into account the peculiarities of each device. The following results are given: linear analytical and nonlinear computer mathematical models of the SP reflecting its properties at different values of displacements of the output link are obtained. The mathematical model of the SP is synthesised on the basis of research of properties of its real elements separately and as an integral tracking system. Scientific novelty of the obtained results consists in the following: a method of element-by-element mathematical description of SPs with subsequent experimental identification of their characteristics; a method of building a universal model of a mechatronic system containing, as a rule, digital and nonlinear elements.

References

1. Arduino Servo Motor Basics and Control, https://makersportal.com/blog/2020/3/14/arduino-servo-motor-control, last accessed 2023/11/20.
2. Tadesse, Y., Subbarao, K., Priya, J.: Realizing a Humanoid Neck with Serial Chain Four-bar Mechanism. Journal of Sntelligent Material Systems and Structures 21(12), 1169–1191 (2010).
3. ArduPilot Copter, Sero, https://ardupilot.org/copter/docs/common-servo.html, last accessed 2023/11/22.
4. Tesfamikael, H.H., Fray, A., Mengsteab, I., Semere, A., Amanuel, Z.: Construction of Mathematical Model of DC Servo Motor Mechanism with PID controller for Electric Wheel Chair Arrangement. Journal of Electronics and Informatics 03(01), 49–60 (2021).
5. Arduino Servo Drives SG90, MG995, MG996: Wiring and Control Schematic, https://arduinomaster.ru/motor-dvigatel-privod/servoprivody-arduino-sg90-mg995-shema-pod-klyuchenie-upravlenie/, last accessed 2023/11/23.
6. Pliuhin, V., Aksonov, O., Tsegelnyk, Y., Plankovskyy, S., Kombarov, V., & Piddubna, L. Design and Simulation of a Servo-Drive Motor Using ANSYS Electromagnetics. Lighting Engineering & Power Engineering 60 (3), 112–123 (2021).
7. Kochuk S. B.: About an integrated approach to the design of small unmanned aerial vehicles. No. 74. Collection of scientific papers "Open information and computer integrated technologies", Kharkiv, KhAI (2016).
8. Shuvu Shang, Ming Yang, Dianguo Xu: Design and Research of Servo Drive System Based on GaN Power Device. 21st International Conference on Electrical Machines and Systems, ICEMS, vol. 21, pp. 1313–1317. KIEE Electrical Machinery and Energy Conversion Systems, Jeju, Korea (South) (2018).
9. Shuai Zhang: Research on servo motor motion control system based on Beckhoff PLC. Journal of Physics Conference Series 1852(2):022002, (2021).
10. Kochuk, S. B., Nikitin A. O.: Practical study of automation objects. Kharkiv, KhAI (2021).
11. Lab 21: servo motor control, https://embedded-lab.com/blog/lab-21-servo-motor-control/, last accessed 2023/11/19.
12. What Is The Working Principle And Internal Structure Of The Servo Drive?, https://www.hybridservos.com/news/work-principle-internal-structure-servo-driver-21504016.html, last accessed 2023/11/19.
13. Kochuk, S., Nguyen, D., Nikitin, A., & Trujillo Torres, R.: Identification of UAV model parameters from flight and computer experiment data. Aerospace Technic and Technology 0(6), 12–22 (2021).
14. Trishch R., Nechuiviter O., Hrinchenko H., Bubela T., Riabchykov M., Pandova I.: Assessment of safety risks using qualimetric methods. MM Science Journal, 6668 -6674 (2023).
15. Trishch, R, Maletska, O, Hrinchenko, H: Development and validation of measurement techniques according to ISO/IEC 17025:2017. In: Proceedings of the 8th International Conference on Advanced Optoelectronics and Lasers, pp. 715–720. Sozopol (2019).